Optics Letters

Three-dimensional Dirac semimetal thin-film absorber for broadband pulse generation in the near-infrared

Yafei Meng,[1] Chunhui Zhu,[1] Yao Li,[1,3] Xiang Yuan,[2] Faxian Xiu,[2] Yi Shi,[1] Yongbing Xu,[1] and Fengqiu Wang[1,*]

[1]School of Electronic Science and Engineering and Collaborative Innovation Center of Advanced Microstructures, Nanjing University, Nanjing 210093, China
[2]State Key Laboratory of Surface Physics and Department of Physics, Collaborative Innovation Center of Advanced Microstructures, Fudan University, Shanghai 200433, China
[3]e-mail: liyao@nju.edu.cn
*Corresponding author: fwang@nju.edu.cn

Received 17 January 2018; accepted 17 February 2018; posted 26 February 2018 (Doc. ID 320009); published 22 March 2018

In this Letter, the transient nonlinear absorption of three-dimensional (3D) topological Dirac semimetal Cd_3As_2 thin film was characterized in the near-infrared band. By performing broadband pump–probe measurements, we experimentally proved that molecular beam epitaxy (MBE) grown Cd_3As_2 exhibits strong and tunable saturable absorption effects across 1–2 μm. By further inserting the Cd_3As_2 film into the cavities of Tm- and Er-doped fiber lasers, we obtained stable mode-locked operations at 1.96 and 1.56 μm. Our results experimentally establish that Cd_3As_2 is a promising broadband saturable absorber (SA) for pulsed lasers in the infrared range.

OCIS codes: (140.3510) Lasers, fiber; (140.3538) Lasers, pulsed; (160.4330) Nonlinear optical materials.

https://doi.org/10.1364/OL.43.001503

Ultra-short pulsed sources in the infrared (IR) have opened up a diverse range of applications from basic research to telecommunications, medicine, and industrial materials processing [1–4]. Passive mode-locking based on a saturable absorber (SA) represents the state-of-the-art technique for obtaining ultra-short pulses [3]. Over the past few decades, various SA materials, e.g., organic dyes, color centers, and transition-metal-doped crystals, have been uncovered [5–7]. However, these materials suffer from toxicity, low durability, and narrow parameter space, leading to compromised laser performance and limited use in certain laser formats. Semiconductor SA mirrors (SESAMs), a breakthrough in the early 1990s [8], represent the first SAs that feature highly flexible parameter customization, as the device fabrication is based on the highly mature and precise thin-film deposition technology, such as molecular beam epitaxy (MBE). It has provided a desirably large parameter space that is needed to greatly upgrade the performance levels of pulsed lasers [9,10]. However, SESAMs have some limitations. Their operation bandwidth is typically within a few hundred nanometers, and they are currently operating under a cutoff wavelength around 3 μm, which prevents their use in broadly tunable lasers and pulsed mid-IR lasers [11].

In the past few years, low-dimensional materials, including carbon nanotubes [12–14], graphene [15–17], topological insulator [18], transition metal dichalcogenides [19,20], etc., have been intensively investigated for ultra-short pulse generation [21,22]. Although they all seem to possess advantages, such as low-cost processing and broad operation bandwidth, the defect-prone exfoliation, placement, and transfer processes inevitably lead to poor repeatability and reliability [23–25]. Furthermore, in terms of optical parameter customization, no strategies in these systems have been developed to rival that of the capabilities of SESAMs [9,26]. Alternative nonlinear optical materials possessing the combined advantages of SESAMs and low-dimensional materials are therefore highly desirable.

Very recently, three-dimensional (3D) Dirac semimetal cadmium arsenide (Cd_3As_2) has been reported to exhibit excellent mid-IR (3–6 μm) saturable absorption properties [27]. On one hand, it has a band structure that is highly similar to graphene, ensuring strong and broadband light–matter interactions [28,29], and, on the other, it comes in the form of optical thin films, where various parameter control strategies for conventional semiconductors can be readily applied. Recently, we have demonstrated that the relaxation times of Cd_3As_2 can be flexibly controlled over an order of magnitude in the mid-IR of 3–6 μm, making it a potential candidate for fabricating SESAM-like broadband SAs [27,30]. Although this material has been successfully used for a mode-locking fiber laser at ~3 μm, up till now, its nonlinear optical properties across the near-IR band, where a number of popular gain materials abound, remains largely unexplored. The multiple band transitions in the near-IR, as opposed to the simple transitions between the two Dirac bands for mid-IR absorption, makes

it also physically interesting to observe potentially interesting intra-band photocarrier dynamics.

In this Letter, by performing broadband pump–probe measurements, we experimentally proved that Cd_3As_2 also exhibits remarkable saturable absorption properties across the 1–2 μm near-IR range. In particular, recovery time of the thin-film absorber can be customized using chromium (Cr) ions doping. Taking advantage of its broadband near-IR saturable absorption, we applied the same Cd_3As_2 thin-film SA in two separate fiber lasers (using Tm- and Er-doped fiber as gain media, respectively). We obtained stable mode-locked operations at 1.96 and 1.56 μm. Our results show that Cd_3As_2 film is a high-performance tunable SA for the near-IR, as well as the mid-IR pulsed lasers.

High-quality Cd_3As_2 thin film with a thickness of 300 nm was grown on mica substrate by MBE [27]. X-Ray diffraction (XRD) of the thin film is shown in Fig. 1(a). A series of peaks can be well resolved and indexed as a {112} crystal plane (the un-indexed peaks come from the mica substrate), meaning good crystallinity of the sample [31]. The Cd_3As_2 sample was mechanically exfoliated from the substrate, and its linear transmission at the wavelength range from 1000 to 2400 nm was measured by Fourier transform IR spectroscopy (VERTEX70, Bruker Inc.). As shown in Fig. 1(b), the transmissions are 30.5%, 41%, 35.5%, and 31% at investigated wavelengths of 1.06, 1.3, 1.56, and 1.96 μm, respectively. The low transmission coefficients are mainly due to the reflection from the film surface [32].

Then, the nonlinear optical properties of the thin-film sample are first characterized in a non-degenerate pump–probe experiment [33]. The experimental setup is shown in Fig. 2(a). The optical source of the experiment is from a high-power Ti:sapphire laser (Libra, Coherent Inc.), which delivers 1 kHz repetition rate, ~100 fs pulse duration pulses at 800 nm. One part of the laser output is used as the pump to excite photocarriers in the sample, and the remaining is fed to an optical parametric amplifier (OPA, Opera Solo, Coherent Inc.) to generate a wavelength-tunable near-IR probe beam. Figures 2(b)–2(e) show transient probe transmission spectra for the Cd_3As_2 sample with four different probe wavelengths at 1.0, 1.3, 1.5, and 2 μm. All of the measured curves exhibit a sharp transmission increase at time zero, indicating that Cd_3As_2 processes saturable absorption over the investigated near-IR spectral range. Meanwhile, fitted by a mono-exponential delay function (black solid lines), the relaxation curves indicate that the SA has a recovery time around 4–5 ps.

Parameter customization plays a key role in enabling high-performance optical switching devices, and this capability has made III–V material-based SESAMs particularly adaptable to various laser formats [34]. It has been proved that flexible

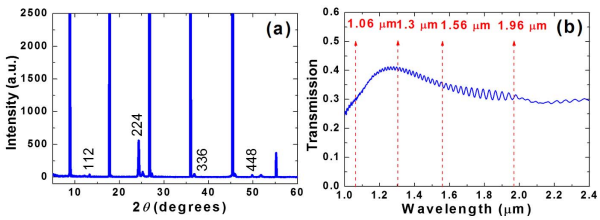

Fig. 1. (a) X-ray diffraction pattern with {112} crystal surface; (b) the linear transmission spectrum of the Cd_3As_2 sample.

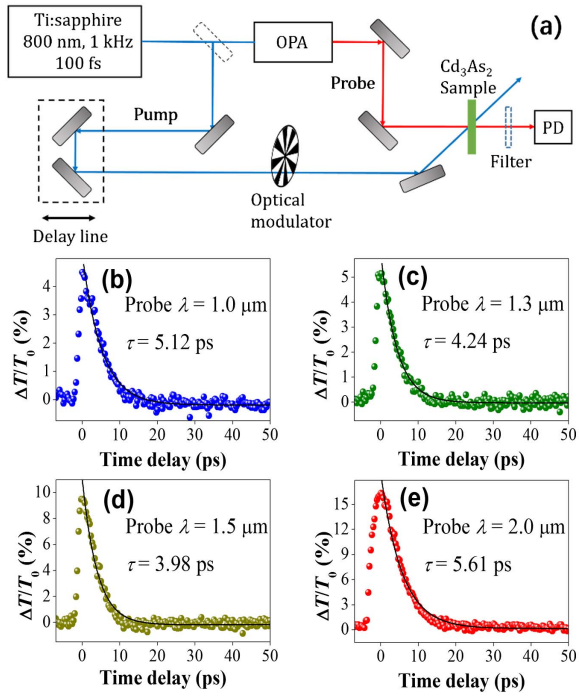

Fig. 2. Pump–probe results. (a) Scheme of the pump–probe experiment; (b)–(e) the transient transmission spectra for Cd_3As_2 thin film with four selected probe wavelengths at 1, 1.3, 1.5, and 2 μm. The pump fluence is about 300 μJ/cm^2.

tuning of Cd_3As_2's relaxation time can be achieved by introducing Cr as a dopant to the films [27]. Here, we focus on the tuning effect at near-IR wavelengths. Figure 3 shows the normalized degenerate ultrafast spectroscopy for Cd_3As_2 samples having different Cr concentrations at a wavelength of 2 μm. It is observed that the decay rate of photoexcited carriers become faster at higher Cr concentrations. The fitted time constants as a function of Cr concentration are summarized in the inset of Fig. 3. Tuning of the photocarrier recovery time down to 500 fs is feasible.

Other nonlinear saturable absorption properties of the Cd_3As_2 film, for example, the modulation depth and saturation intensity, are also very important for mode-locked and *Q*-switched lasers. Then, the typical two arms transmission measurement was employed to characterize these parameters [35].

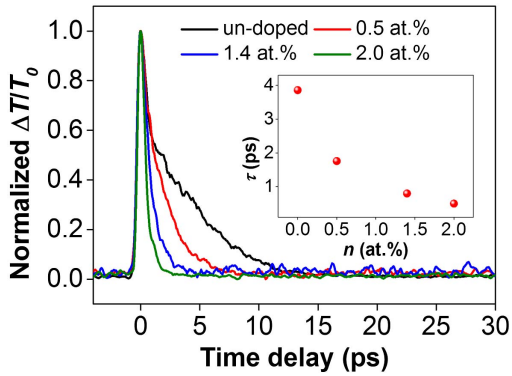

Fig. 3. Normalized degenerate transient spectra for Cd_3As_2 samples having different Cr concentrations.

The prepared Cd_3As_2 film (~300 nm thick, undoped) was sandwiched between two fiber ferrule ends. A homemade passively mode-locked Tm/Ho fiber laser (with a center wavelength of ~1.96 μm, a repetition rate of 50 MHz) was amplified by a commercial thulium-doped fiber amplifier (TDFA-2000, NPI Lasers Inc.) for obtaining high peak power to sufficiently saturate the Cd_3As_2 sample. The maximum power after amplification is ~20 mW, and the output pulse width is 700 fs. A typical nonlinear absorption curve at 1967 nm is shown in Fig. 4(a). The modulation depth and saturation intensity were calculated to be 3.5% and 12 MW/cm^2, respectively. By the same way, the nonlinear saturable absorption properties around the 1.5 μm wavelength band were also measured using an Er-doped femtosecond fiber laser (Rainbow 1550, NPI Lasers Inc.). The pulse duration of the laser is 340 fs. As shown in Fig. 4(b), the modulation depth and the saturation intensity are 5.1% and 67 MW/cm^2, respectively. As there is partial reflection from the surface of the samples, we can use a reflective SESAM-like structure and put the absorber in a resonant Fabry–Perot cavity to improve the nonlinear parameters, such as non-saturable loss and modulation depth.

Due to the lack of suitable laser sources, we cannot directly measure the saturation parameters of Cd_3As_2 film at the 1 μm wavelength. Besides, the damage threshold of Cd_3As_2 film at 2 μm is tested to be ~10 GW/cm^2 by monitoring the sample's transmittance as a function of illumination intensity [27]. This high damage theshold indicates that this material is robust under high-power lasing and stable for long term running.

In order to demonstrate that Cd_3As_2 can be used as SA for pulsed lasers at the abovementioned wavelengths, we designed a 1.96 μm Tm–Ho co-doped fiber laser (THDFL) and a 1.56 μm Er-doped fiber laser (EDFL) passively modulated by a Cd_3As_2 thin-film SA. The experimental setup is shown in Fig. 5. The two cavities are based on almost the same structure.

First, we incorporated the Cd_3As_2-SA (~300 nm thick, undoped) in a Tm–Ho co-doped ring cavity fiber laser. The amplified 1.56 μm pump is coupled into the cavity via a 1550/2000 nm wavelength-division multiplexer (WDM). A 2 m Tm/Ho co-doped fiber (TH512, CorActive) with 9/125 core/cladding geometry is used as the gain medium. An inline polarization insensitive isolator is spliced after the gain fiber and ensures unidirectional operation of the oscillator. The output is coupled from the laser cavity through a 50/50 coupler. The pigtail fiber of all the passive components is SMF-28, and the total fiber length of the cavity is 8.5 m. The laser starts mode-locking with a pump threshold of 285 mW. Under this pump level, the average output power is 4.9 mW. Good

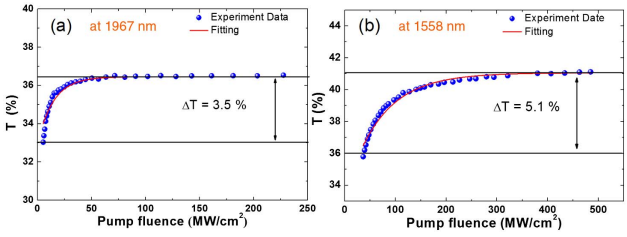

Fig. 4. Nonlinear absorption curves of Cd_3As_2-SA. The blue balls (color online) are the experimental data, and the red line is the fitting result.

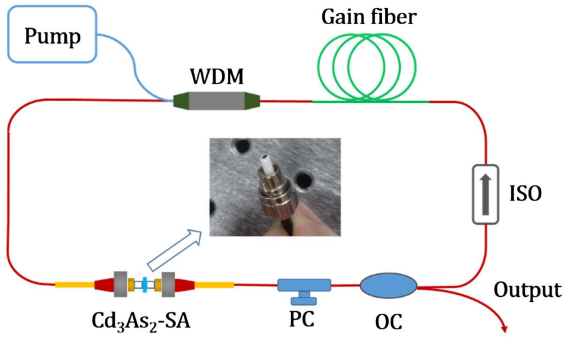

Fig. 5. Schematic of the pulsed fiber laser. WDM, wavelength-division multiplexer; ISO, isolator; OC, output coupler; PC, polarization controller.

self-starting performance is maintained very well beyond the pump threshold power.

Figure 6(a) shows the mode-locking pulse train detected by a high-speed photodiode (EOT-5000). The time interval between adjacent pulses is 43 ns, which matches well with the fundamental repetition rate of 23.22 MHz. Figure 6(b) shows the RF spectrum of the output pulses measured by a signal analyzer (R&S, FSV 30). The RF spectrum shows a signal-to-noise ratio of 70 dB at the fundamental rate of ~23.22 MHz, and no amplitude modulation is observed within 1 GHz band (shown in the inset), indicating the mode-locked pulse is very stable. Figure 6(c) shows the optical spectra of the mode-locked pulses by an optical spectrum analyzer (OSA, Yokogawa AQ6375). The output spectrum is centered at 1968.5 nm with a 3 dB bandwidth of 3.5 nm. The Kelly sidebands are clearly visible on the optical spectrum, as the mode-locked laser is working in the soliton regime. The corresponding pulse duration is analyzed by a mid-IR autocorrelator (Femtochrome, FR-103XL). The full width at half-maximum (FWHM) of the trace is 2.1 ps, as shown in Fig. 6(d). If a sech^2 pulse profile is assumed, the soliton pulse duration is calculated to be 1.36 ps. The time-bandwidth product (TBP) is 0.36, which is close to the transform limited value of 0.315.

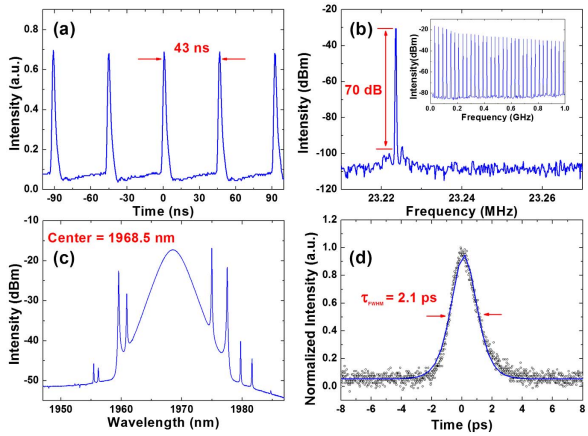

Fig. 6. Typical mode-locked characteristics of the 1.96 μm THDFL. (a) The typical oscilloscope trace. (b) RF output spectrum; inset: broadband RF output spectrum. (c) Output optical spectrum. (d) Autocorrelation trace of the mode-locked pulses.

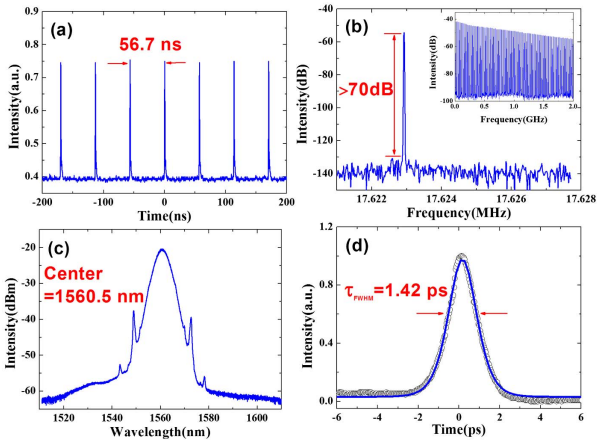

Fig. 7. Typical characteristics of the mode-locked EDFL at 1.56 μm. (a) The typical oscilloscope trace, (b) RF spectrum; inset: broadband RF spectrum. (c) Typical output optical spectrum, (d) autocorrelation trace of the mode-locked pulses.

To further prove the mode-locking ability for shorter wavelength lasers, the same Cd_3As_2-SA was inserted into an Er-doped ring cavity fiber laser. The pump source is a 980 nm laser diode. A 1 m Er-doped fiber (Er80-4/125, Liekki) is used as the gain medium. The total length of the mode-locked Er fiber laser is 11.2 m. The experimental results are shown in Figs. 7(a)–7(d). The laser starts mode-locking with the pump threshold of 30 mW, and the average output power is 0.7 mW. Similar with the performance of the THDFL, a high signal-to-noise ratio of 70 dB was clearly observed at the fundamental rate of ~17.6 MHz, demonstrating that the mode-locking state was quite stable. The laser spectrum is centered at 1560 nm with a 3 dB bandwidth of 4.8 nm, and the pulse duration is measured to be 0.92 ps.

In summary, we have experimentally verified that 3D topological Dirac semimetal Cd_3As_2 thin-film exhibits ultrafast nonlinear absorption at the near-IR band. The modulation depth and saturable intensity of the Cd_3As_2-film SA measured at 1.96 and 1.56 μm wavelengths are 3.5% and 12 MW/cm^2, 5.1% and 67 MW/cm^2, respectively. For the first time, to the best of our knowledge, we obtained stable mode-locked fiber lasers at 1.96 and 1.56 μm by using this emerging SA device. Our results establish Cd_3As_2 film as a promising SA device for wideband and tunable mode-locked lasers across the near- and mid-IR wavelength range.

Funding. National Key R&D Program of China (2017YFA0206304); National Basic Research Program of China (2014CB921101); National Natural Science Foundation of China (NSFC) (61775093, 61378025, 61427812); Natural Science Foundation of Jiangsu Province (BK20170012, BK20140612); "Jiangsu Shuangchuang Team" Program.

REFERENCES

1. V. S. Letokhov, Nature **316**, 325 (1985).
2. F. Dausinger, H. Lubatschowski, and F. Lichtner, *Femtosecond Technology for Technical and Medical Applications* (Springer, 2004).
3. U. Keller, Nature **424**, 831 (2003).
4. K. Schütze, H. Pösl, and G. Lahr, Cell. Mol. Biol. **44**, 735 (1998).
5. A. J. DeMaria, D. A. Stetser, and H. Heynau, Appl. Phys. Lett. **8**, 174 (1966).
6. Y. Kalisky, Prog. Quantum Electron. **28**, 249 (2004).
7. M. B. Camargo, R. D. Stultz, M. Birnbaum, and M. Kokta, Opt. Lett. **20**, 339 (1995).
8. U. Keller, D. A. B. Miller, G. D. Boyd, T. H. Chiu, J. F. Ferguson, and M. T. Asom, Opt. Lett. **17**, 505 (1992).
9. E. Lugagne Delpon, J. L. Oudar, N. Bouché, R. Raj, A. Shen, N. Stelmakh, and J. M. Lourtioz, Appl. Phys. Lett. **72**, 759 (1998).
10. U. Keller, K. J. Weingarten, F. X. Kartner, D. Kopf, B. Braun, I. D. Jung, R. Fluck, C. Honninger, N. Matuschek, and J. Aus der Au, IEEE J. Sel. Top. Quantum Electron. **2**, 435 (1996).
11. BATOP GmbH company, "SAM product list," http://www.batop.de/products/saturable-absorber/saturable-absorber-mirror/saturable-absorber-mirror.html.
12. M. A. Solodyankin, E. D. Obraztsova, A. S. Lobach, A. I. Chernov, A. V. Tausenev, V. I. Konov, and E. M. Dianov, Opt. Lett. **33**, 1336 (2008).
13. V. Scardaci, A. G. Rozhin, P. H. Tan, F. Wang, I. H. White, W. I. Milne, and A. C. Ferrari, Phys. Status Solidi B **244**, 4303 (2007).
14. F. Wang, A. G. Rozhin, V. Scardaci, Z. Sun, F. Hennrich, I. H. White, W. I. Milne, and A. C. Ferrari, Nat. Nanotechnol. **3**, 738 (2008).
15. Q. Bao, H. Zhang, Y. Wang, Z. Ni, Y. Yan, Z. X. Shen, K. P. Loh, and D. Y. Tang, Adv. Funct. Mater. **19**, 3077 (2009).
16. M. Zhang, E. J. R. Kelleher, F. Torrisi, Z. Sun, T. Hasan, D. Popa, F. Wang, A. C. Ferrari, S. V. Popov, and J. R. Taylor, Opt. Express **20**, 25077 (2012).
17. F. Wang, F. Torrisi, Z. Jiang, D. Popa, T. Hasan, Z. Sun, W. Cho, and A. C. Ferrari, in *Conference on Laser and Electro-Optics: Science and Innovations* (Optical Society of America, 2012), paper JW2A.72.
18. M. Jung, J. Lee, J. Koo, J. Park, Y. W. Song, K. Lee, S. Lee, and J. H. Lee, Opt. Express **22**, 7865 (2014).
19. Z. Tian, K. Wu, L. Kong, N. Yang, Y. Wang, R. Chen, W. Hu, J. Xu, and Y. Tang, Laser Phys. Lett. **12**, 065104 (2015).
20. M. Jung, J. Lee, J. Park, J. Koo, Y. M. Jhon, and J. H. Lee, Opt. Express **23**, 19996 (2015).
21. J. Sotor, G. Sobon, M. Kowalczyk, W. Macherzynynski, P. Paletko, and K. M. Abramski, Opt. Lett. **40**, 3885 (2015).
22. S. Lu, L. Miao, Z. Guo, X. Qi, C. Zhao, H. Zhang, S. Wen, D. Tang, and D. Fan, Opt. Express **23**, 11183 (2015).
23. G. Sobon, Photon. Res. **3**, A56 (2015).
24. R. Going, D. Popa, F. Torrisi, Z. Sun, T. Hasan, F. Wang, and A. C. Ferrari, Physica E **44**, 1078 (2012).
25. G. Zhu, X. Zhu, F. Wang, S. Xu, Y. Li, X. Guo, K. Balakrishnan, R. A. Norwood, and N. Peyghambarian, IEEE Photon. Technol. Lett. **28**, 7 (2016).
26. M. Haiml, U. Siegner, F. Morier-Genoud, U. Keller, M. Luysberg, R. C. Lutz, P. Specht, and E. R. Weber, Appl. Phys. Lett. **74**, 3134 (1999).
27. C. Zhu, F. Wang, Y. Meng, X. Yuan, F. Xiu, H. Luo, Y. Wang, J. Li, X. Lv, L. He, Y. Xu, J. Liu, C. Zhang, Y. Shi, R. Zhang, and S. Zhu, Nat. Commun. **8**, 14111 (2017).
28. Q. Wang, C. Z. Li, S. Ge, J. G. Li, W. Lu, J. Lai, X. Liu, J. Ma, D. P. Yun, Z. M. Liao, and D. Sun, Nano Lett. **17**, 834 (2017).
29. W. Lu, S. Ge, X. Liu, H. Lu, C. Li, J. Lai, C. Zhao, Z. Liao, S. Jia, and D. Sun, Phys. Rev. B **95**, 024303 (2017).
30. C. Zhu, X. Yuan, F. Xiu, C. Zhang, Y. Xu, R. Zhang, Y. Shi, and F. Wang, Appl. Phys. Lett. **111**, 091101 (2017).
31. Y. Liu, C. Zhang, X. Yuan, T. Lei, C. Wang, D. D. Sante, A. Narayan, L. He, S. Picozzi, S. Sanvito, R. Che, and F. Xiu, NPG Asia Mater. **7**, e221 (2015).
32. A. A. El-Shazly, H. S. Soliman, D. A. Abd El-Hady, and H. E. A. El-Sayed, Vacuum **47**, 53 (1996).
33. S. Xu, F. Wang, C. Zhu, Y. Meng, Y. Liu, W. Liu, J. Tang, K. Liu, G. Hu, R. C. T. Howe, T. Hasan, R. Zhang, Y. Shi, and Y. Xu, Nanoscale **8**, 9304 (2016).
34. A. Rutz, V. Liverini, R. Grange, M. Haiml, S. Schön, and U. Keller, J. Cryst. Growth **301**–302, 570 (2007).
35. J. Du, Q. Wang, G. Jiang, C. Xu, C. Zhao, Y. Xiang, Y. Chen, S. Wen, and H. Zhang, Sci. Rep. **4**, 6346 (2014).